Ag₂O and NiO Decorated CuFe₂O₄ with Enhanced Photocatalytic Performance to Improve the Degradation Efficiency of Methylene Blue

Lu Liu [1,2,*]**, Nan Hu** [1,2,*]**, Yonglei An** [3,4]**, Xingyuan Du** [3,4]**, Xiao Zhang** [1]**, Yan Li** [1]**, Yan Zeng** [1] **and Zheng Cui** [5]

[1]   School of Energy and Power Engineering, Changchun Institute of Technology, Changchun 130012, China; zhangx049@nenu.edu.cn (X.Z.); moon471285743@126.com (Y.L.); zengyan@ccit.edu.cn (Y.Z.)

[2]   Jilin Province S&T Innovation Center for Physical Simulation and Security of Water Resources and Electric Power Engineering, Changchun Institute of Technology, Changchun 130012, China

[3]   Key Laboratory of Groundwater Resources and Environment, Jilin University, Ministry of Education, Changchun 130021, China; anyonglei85@jlu.edu.cn (Y.A.); duxy19@mails.jlu.edu.cn (X.D.)

[4]   Jilin Provincial Key Laboratory of Water Resources and Environment, Jilin University, Changchun 130021, China

[5]   State Key Laboratory of Superhard Materials, College of Physics, Jilin University, Changchun 130012, China; cuizheng18@mails.jlu.edu.cn

*   Correspondence: liulu@ccit.edu.cn (L.L.); hunan@ccit.edu.cn (N.H.)

check for updates

Abstract: Dye wastewater is a serious threat to human health and life. It is an important task for researchers to treat it efficiently. Among many treatment methods, the photo-Fenton method can rapidly degrade organic pollutants. In this study, a ternary photocatalyst, Ag₂O-NiO/CuFe₂O₄, was prepared and applied for a photo-Fenton reaction to degrade methylene blue (MB). MB had the best degradation effect when 10 mg of the catalyst were used in an 80 mL reaction system for measurement. The degradation rate of MB was up to 96.67% in 60 min with a high degradation rate constant $k = 5.67 \times 10^{-2} \text{min}^{-1}$. The total organic carbon (TOC) degradation rate was 78.64% with a TOC degradation rate constant of $k = 2.57 \times 10^{-2} \text{min}^{-1}$. Therefore, this study fully proves that Ag₂O-NiO/CuFe₂O₄ can catalyze the photo-Fenton reaction and effectively degrade MB.

1. Introduction

With the rapid development of global industry, the problem of water pollution has become more and more severe. Organic dyes based on heterocyclic aromatic/aromatic-azo compounds are highly toxic, carcinogenic, and difficult to degrade [1,2]. Methylene blue (MB) mainly comes from the printing and dyeing industry [3]. MB can prevent sunlight from entering water and therefore affects the growth of aquatic organisms [4]. Furthermore, MB can cause eye burns and may even lead to permanent damage. If MB is taken into the body, it will cause a burning sensation and vomiting. Therefore, the treatment of dye wastewater has become an urgent problem. Unfortunately, traditional wastewater treatment processes (microbial degradation) cannot efficiently decompose MB.

In recent years, researchers have proposed many new technologies, such as adsorption, condensation, photocatalysis, electrocatalysis, and the photo-Fenton process [5–8]. Solar energy is an inexhaustible clean energy source that can be used to degrade MB and other dyes. Due to the economics of solar energy, photocatalysis is considered one of the most promising methods. Many semiconductor materials can decompose toxic organic compounds into non-toxic inorganic

compounds under light irradiation. Various semiconductors have been developed as photocatalysts, including $CuFe_2O_4$, TiO_2, CdS, Bi_2O_3, Ag_2O, NiO, and g-C_3N_4 and so on [9–12]. Copper ions and iron ions can participate in the photo-Fenton reaction [13]. Therefore, $CuFe_2O_4$ can also trigger the photo-Fenton reaction.

Among many photocatalysts, $CuFe_2O_4$ has attracted wide attention because of its suitable energy band structure, high chemical stability, thermal stability and low toxicity [14]. In addition, $CuFe_2O_4$ has magnetic properties that makes it easy to recycle [15,16]. It will not cause secondary pollution and can be widely used in heterogeneous catalysis. $CuFe_2O_4$ has a relatively narrow band gap [17] that can absorb visible light. In order to increase its absorption rate of visible light, it is often prepared into a micro-nano structure [18,19]. The surface of the structure produces defect energy levels and surface energy levels during the preparation process, thereby providing a recombination center for photo-generated electron-holes [20,21]. Then, the lifetime of electrons and holes is reduced, i.e., the photocatalytic efficiency is reduced. Therefore, a single transition metal oxide used for the photocatalytic degradation of MB cannot meet the needs of practical applications. At present, researchers have made many efforts to improve the photocatalytic properties of materials, such as noble metal loading, metal doping, and coupling with other semiconductors (MoS_2, Co_3O_4, NiO, WO_3, etc.) [9,22–24]. The latest literature has reported that mixed transition metal oxides (CuO/Fe_3O_4, $CuO/MnFe_2O_4$, γ-Fe_2O_3/Mn_3O_4, and CoO-CuO) not only have excellent catalytic performance but also maintain excellent stability [24–26]. Therefore, the combination of $CuFe_2O_4$ and other semiconductors would increase the photo-Fenton reaction rate.

Ag_2O and NiO are often used in photocatalysis research. Though it is a narrow-band gap semiconductor, Ag_2O is rarely used as the main catalyst, but it is used as a co-catalyst due to the instability of its photocatalytic reaction and its high carrier recombination rate [23,27]. NiO is a wide band gap semiconductor with important electronic, chemical, and electrical properties [28]. NiO can only absorb ultraviolet light, so its utilization rate of sunlight is low. It is the best choice to combine NiO with other semiconductor materials to improve its photocatalytic activity.

Based on above introduction, the hydrothermal method and calcination were used to prepare an Ag_2O-NiO/$CuFe_2O_4$ ternary catalyst, which showed an excellent photocatalytic performance under sunlight. Within 60 min of photocatalytic degradation in photo-Fenton system, the removal rate of MB was 96.67%. The degradation mechanism of MB in this study was analyzed according to its characterization and catalytic performance.

2. Material and Methods

2.1. Chemicals

Copper sulfate pentahydrate ($CuSO_4 \cdot 5H_2O$, analytical reagent (AR)), ferric chloride hexahydrate ($FeCl_3 \cdot 6H_2O$, AR), nickel acetate tetrahydrate ($C_4H_6NiO_4 \cdot 4H_2O$, AR), silver sulfate (Ag_2SO_4, AR), sodium hydroxide (NaOH, AR), methylene blue (MB, AR), 30.0% hydrogen peroxide (H_2O_2, AR), absolute ethanol (EtOH, C_2H_5OH, AR), and t-butanol (TBA, $(CH_3)_3COH$, AR) were purchased from Sinopharm Chemical Reagent (Shanghai, China) and were used as received without further purification.

2.2. Synthesis and Characterization of Ag_2O-$CuFe_2O_4$/NiO

In 200 mL deionized water, 3.210 g $CuSO_4 \cdot 5H_2O$ and 2.705 g $FeCl_3 \cdot 6H_2O$ were fully dissolved under magnetic stirring; this is marked as solution A. Additionally, a 100 mL NaOH solution was prepared with a final pH of 9; this is marked as solution B. We dropwise added solution A to solution B under magnetic stirring, and we kept the pH of the mixture at 9 from beginning to end by adding 1.0 M NaOH, thus generating a black suspension. Then, the suspension was evaporated and concentrated to 60 mL at 60 °C under magnetic stirring. The 60 mL concentrated suspension was poured into a stainless steel reactor and placed in a 100 °C oven for 10 h. Subsequently, the concentrated suspension was centrifuged and dried to obtain a black powder, which is denoted as powder C. To remove undesired

soluble ions such as Na^+, SO_4^{2-} and Cl^-, powder C was washed with deionized water and then centrifuged three times; then, precipitate powder C was dried in a 60 °C oven overnight. Then, 0.117 g of Ag_2SO_4 and 0.031 g of $C_4H_6O_4Ni \cdot 4H_2O$ were dissolved in 20 mL of deionized water, and all of black powder C was poured in; this is denoted as mixture M. Mixture M was tempestuously stirred at room temperature for 2 h to make powder C fully and uniformly contact Ag^+ and Ni^{2+}. Then, mixture M was dried at 60 °C under magnetic stirring until the deionized water completely evaporated. We then put the residual solid mixture M into a muffle furnace for high-temperature calcination in an air atmosphere. The detailed process of sample preparation is shown in Figure 1. Figure S1 shows the MB degradation with the samples calcined at different temperatures. It can be found from Figure S1 that the sample calcined at 650 °C had the best degradation effect of MB, so the calcination temperature of all samples used in this study was 650 °C and the sample was coded as Ag_2O-$NiO/CuFe_2O_4$. The molar ratio among Ag_2O, NiO, and $CuFe_2O_4$ was calculated as 3:1:40 in Ag_2O-$NiO/CuFe_2O_4$. For control experiments, a sample without the addition of Ag_2SO_4 and $C_4H_6O_4Ni \cdot 4H_2O$ was also prepared by directly calcining powder C; this is coded as $CuFe_2O_4$.
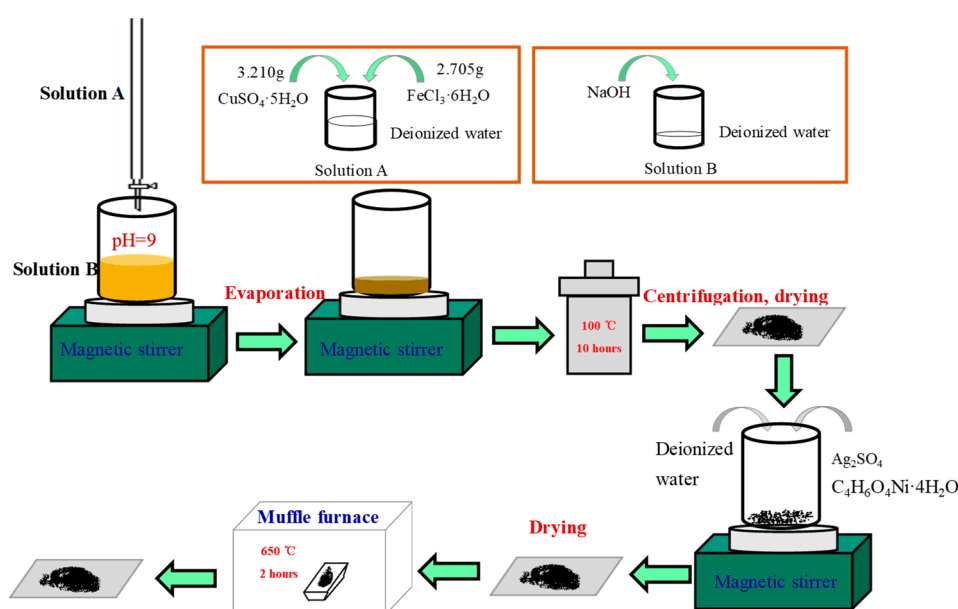

Figure 1. The schematic illustration of the synthetic process of Ag_2O-$NiO/CuFe_2O_4$.

The phase composition and crystal structure of Ag_2O-$NiO/CuFe_2O_4$ were analyzed by transmission electron microscopy (TEM) with a JEM2100 (JEOL, Tokyo, Japan) and X-ray diffraction (XRD) with an XRD-6000 (Shimadzu, Kyoto, Japan) with the radiation ($\lambda = 1.5406$ Å) in the range of 2θ from 10° to 70° and a 1°/min scanning rate.

2.3. Photodegradation Experiments

The photocatalytic performance of Ag_2O-$NiO/CuFe_2O_4$ was evaluated with MB. A 500 W Xe lamp (GXZ500, Shanghai Jiguang special lighting electric appliance factory, Shanghai, China) was used as the simulated sunlight. The distance from the lamp to the MB suspension liquid level was 15 cm. As is typical, 10.0 mg of Ag_2O-$NiO/CuFe_2O_4$ and 100 μL of H_2O_2 were simultaneously added into an aqueous MB solution (80 mL, 10 mg/L), and then the MB photocatalytic degradation experiment was carried out under the irradiation of the Xe lamp. At a certain time interval, a 3 mL suspension was withdrawn from the reaction and subjected to centrifugation. In addition, the same reaction mixture was magnetically stirred in the dark to compare the results irradiated by the Xe lamp. The MB concentration was determined by a UV-VIS spectrophotometer (UV-1240 Shimadzu, Kyoto, Japan) at the wavelength of 664 nm. The total organic carbon (TOC, mg/L) of the MB solution was determined by a TOC analyzer (SSM-5000A Shimadzu, Kyoto, Japan) during the photocatalytic

degradation process. To reveal the photocatalytic mechanism, typical radical scavengers such as EtOH and TBA were used in reactions to verify the active species. We used the same method to analyze the photo-Fenton performance of $CuFe_2O_4$, $NiO/CuFe_2O_4$, and $Ag_2O/CuFe_2O_4$ as the controls. The effects of $NiO/CuFe_2O_4$ and $Ag_2O/CuFe_2O_4$ on MB degradation are shown in Figure S2.

The degradation efficiency of MB can be calculated by Equation (1) [29]:

$$\text{Degradation (\%)} = (1 - C/C_0) \times 100\% \tag{1}$$

where C and C_0 represent the concentration of MB at time t and the pristine concentration of MB, respectively.

In this study, Equation (2) [30] was used to analyze the pseudo-first-order dynamics.

$$-\ln(C/C_0) = kt \tag{2}$$

where k is the apparent reaction rate constant (min^{-1}).

3. Results and Discussion

3.1. Characterization of the Synthesized Ag$_2$O-NiO/CuFe$_2$O$_4$

The phase composition and crystal structure of the sample studied by XRD are shown in Figure 2. The XRD data proved that the material contained three components: Ag_2O, NiO, and $CuFe_2O_4$. The 18.55°, 30.18°, 35.65°, 44.70°, and 65.01° diffraction peaks appeared in the $CuFe_2O_4$ and Ag_2O-$NiO/CuFe_2O_4$ samples. They corresponded to the (101), (112), (211), (202), (220), and (400) crystal planes of $CuFe_2O_4$ (PDF card No.72-1174), respectively. The 32.74° and 53.75° diffraction peaks in Ag_2O-$NiO/CuFe_2O_4$ corresponded to the (111) and (220) crystal planes of Ag_2O (PDF card No.12-793), respectively. The 37.29° and 62.67° diffraction peaks in Ag_2O-$NiO/CuFe_2O_4$ corresponded to the (101) and (110) crystal planes of the NiO phase (PDF card No.44-1159), respectively. These results could convincingly verify the existence of Ag_2O and NiO in Ag_2O-$NiO/CuFe_2O_4$. Therefore, it was proven that Ag_2O, NiO, and $CuFe_2O_4$ were the main components in the sample and the as-prepared Ag_2O-$NiO/CuFe_2O_4$ was synthesized successfully.
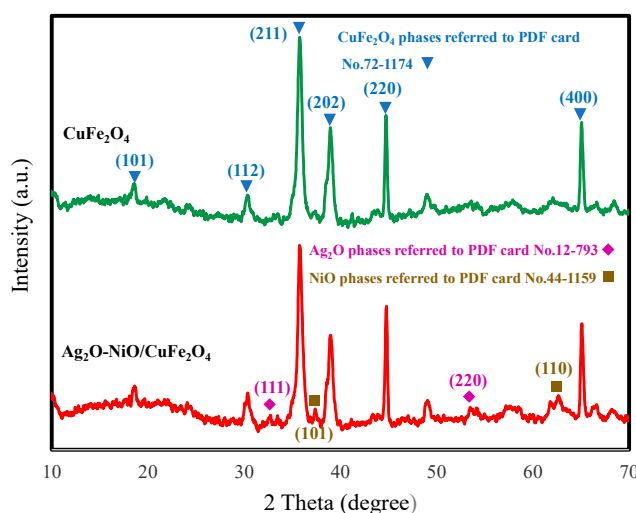

Figure 2. XRD patterns of $CuFe_2O_4$ and Ag_2O-$NiO/CuFe_2O_4$.

The morphology of Ag_2O-$NiO/CuFe_2O_4$ was characterized and analyzed by TEM, as shown in Figure 3. In Figure 3b, the crystal lattice fringe of the sample can be clearly seen, which fully proves that the sample had an excellent crystallinity within a certain size range that was conducive to carrier transmission. Figure 3c–e shows the enlargements of the corresponding square areas in Figure 3b.

The measured lattice plane spacings were 0.48, 0.249, and 0.205 nm, corresponding to the (101), (211), and (220) crystal planes of $CuFe_2O_4$ (PDF card No.72-1174), respectively, which was consistent with the results of XRD. Due to the small proportion of Ag^+ and Ni^{2+} doping, Ag_2O and NiO nanoparticles were not found in the field of TEM.
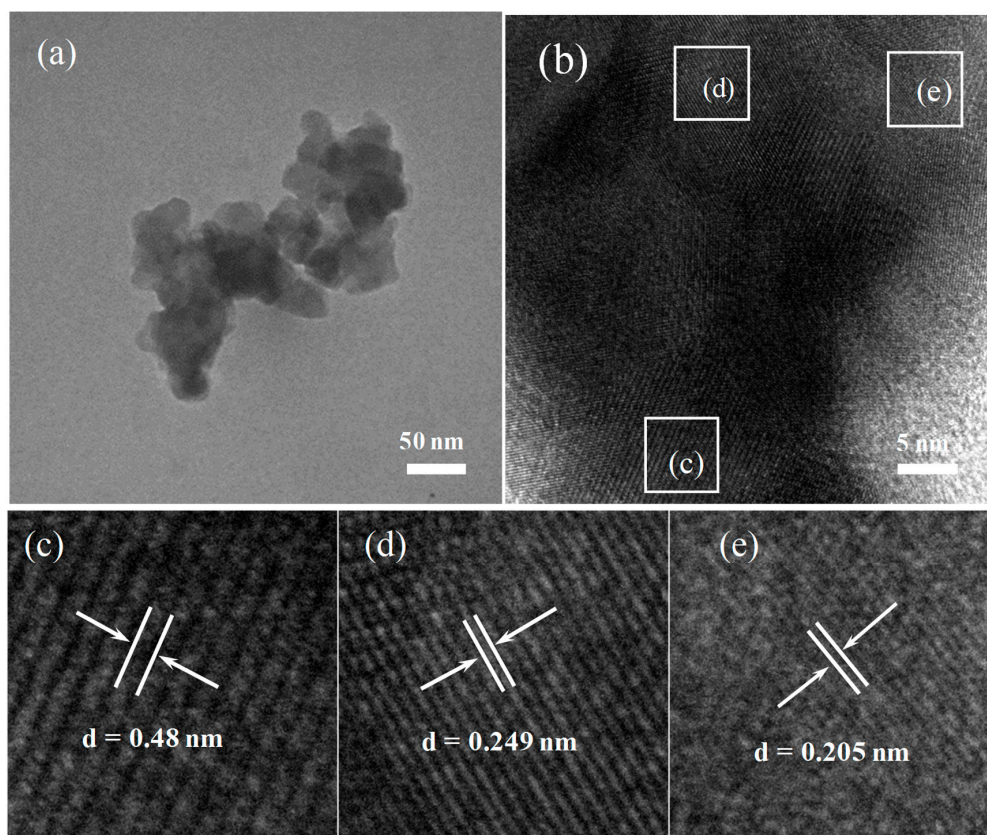

Figure 3. (**a**) TEM image of Ag_2O-NiO/$CuFe_2O_4$; (**b**) High Resolution Translation Electron Microscopy (HRTEM) image of Ag_2O-NiO/$CuFe_2O_4$; (**c–e**) show the enlargements of the corresponding square areas in Figure 3b.

3.2. MB Degradation

The catalytic activity of synthetic nano-material Ag_2O-NiO/$CuFe_2O_4$ was analyzed by observing the degradation of MB in the water phase under simulated sunlight irradiation. The degradation efficiency of MB with different catalysts is shown in Figure 4. In a typical experiment, the solid catalyst dosage was 10 mg and the H_2O_2 dosage was 100 µL, both of which were simultaneously added to an 80 mL MB aqueous solution. Figure 4a shows the degradation of MB by Ag_2O-NiO/$CuFe_2O_4$/H_2O_2 in the dark. Meanwhile, the MB degradation by $CuFe_2O_4$, $CuFe_2O_4$/H_2O_2, H_2O_2, and Ag_2O-NiO/$CuFe_2O_4$ were also compared. The MB removal in each curve decreased within 60 min, and the degradation efficiency of Ag_2O-NiO/$CuFe_2O_4$/H_2O_2 was the highest. However, the removal rate of MB was only 8.60%, and the degradation rate constant was $k = 1.50 \times 10^{-3} min^{-1}$. The removal rate of $CuFe_2O_4$/H_2O_2 on MB was 7.30%, and the degradation rate constant was $k = 3.34 \times 10^{-4} min^{-1}$. The degradation efficiency of pure H_2O_2 was slightly lower than that of Ag_2O-NiO/$CuFe_2O_4$/H_2O_2 and $CuFe_2O_4$/H_2O_2. However, in the comparative experiment without H_2O_2, the MB removal rates of Ag_2O-NiO/$CuFe_2O_4$ and $CuFe_2O_4$ were only 1.98% and 1.04%, respectively. Therefore, it can be seen from these studies that Ag_2O-NiO/$CuFe_2O_4$ and $CuFe_2O_4$ decreased the concentration of MB in the dark due to the small amount of adsorption on the surface of nanomaterials. H_2O_2 could degrade dyes, but the degradation efficiency was low. Figure 4c depicts the MB degradation under simulated sunlight irradiation. Figure 4d shows that Ag_2O-NiO/$CuFe_2O_4$/H_2O_2 had the highest pseudo-first-rate kinetic

constant. Ag$_2$O-NiO/CuFe$_2$O$_4$ and CuFe$_2$O$_4$ could catalyze the degradation of MB with H$_2$O$_2$, the MB removal rates were as high as 96.67% and 57.88%, respectively, and the corresponding degradation rate constants were $k = 5.67 \times 10^{-2}$ and $k = 1.44 \times 10^{-2}$ min^{-1}, respectively. With the assistance of Ag$_2$O-NiO/CuFe$_2$O$_4$, the MB degradation rate constant with H$_2$O$_2$ under simulated sunlight irradiation was two orders of magnitude higher than that in the dark. Therefore, it was proven that we had successfully synthesized a photocatalytic material that efficiently degraded MB. In CuFe$_2$O$_4$, the Cu valence is +2 and the Fe valence is +3. In this study, Fe^{3+} was reduced to Fe^{2+} by photoelectrons. Cu^{2+} and Fe^{2+} can react with H$_2$O$_2$ to produce OH, which can efficiently degrade MB. This process is called the Fenton reaction. Under solar irradiation, the catalytic effect of the catalyst is improved, and this process is called the photo-Fenton reaction. The degradation of MB by Ag$_2$O-NiO/CuFe$_2$O$_4$ and H$_2$O$_2$ under simulated sunlight irradiation was a photo-Fenton reaction.
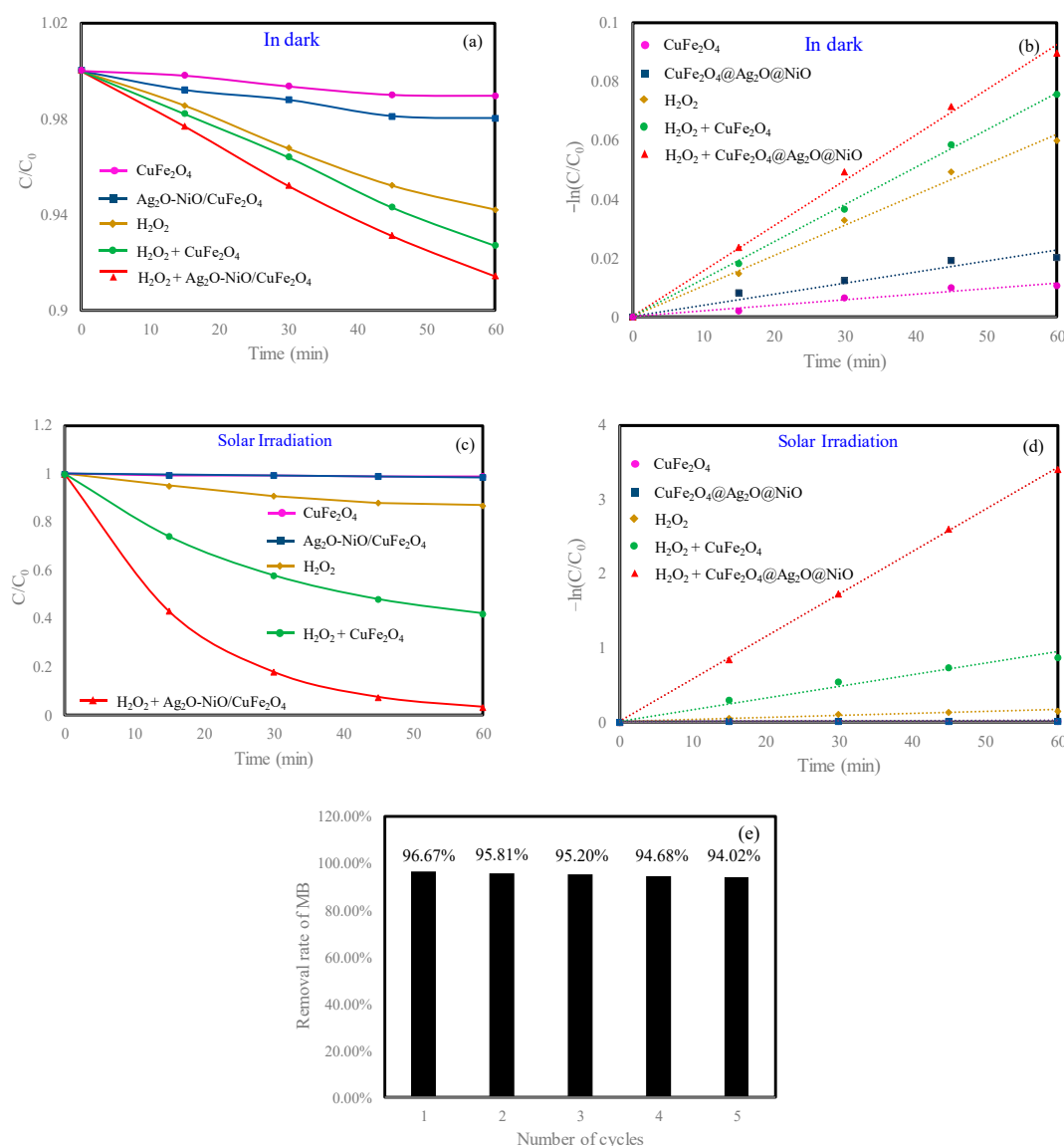

Figure 4. (**a**) Degradation of methylene blue (MB) with different catalysts in the dark; (**b**) the pseudo-first-order reaction kinetics for MB degradation with different catalysts in the dark; (**c**) photocatalytic degradation of MB with different composite photocatalysts under simulated solar irradiation; (**d**) the pseudo-first-order reaction kinetics for MB degradation with different composite photocatalysts under simulated solar irradiation; (**e**) percentage decrease in catalytic efficiency of Ag$_2$O-NiO/CuFe$_2$O$_4$ for five cycles. Initial MB concentration: 10 mg/L. Initial H$_2$O$_2$ concentration: 416 mg/L.

In order to investigate the reuse potential of our photo-Fenton catalyst, Ag_2O-$NiO/CuFe_2O_4$ was collected after each degradation experiment via centrifugation. After deionized water washing and drying at 60 °C, Ag_2O-$NiO/CuFe_2O_4$ was reused as a reactive catalyst for MB degradation under the same experimental conditions, and the results are shown in Figure 4e. The photocatalyst used for the fifth time could still efficiently degrade MB in the aqueous phase, and the removal rate of MB was still as high as 94.02%.

The total organic carbon (TOC) of the MB solution was determined during the experiment. The TOC removal rate and the removal rate constant of Ag_2O-$NiO/CuFe_2O_4$ were 78.64% and $k = 2.57 \times 10^{-2} min^{-1}$ within 60 min, respectively, as shown in Figure 5. The TOC results suggested that Ag_2O-$NiO/CuFe_2O_4/H_2O_2$ could effectively mineralize MB under solar irradiation.
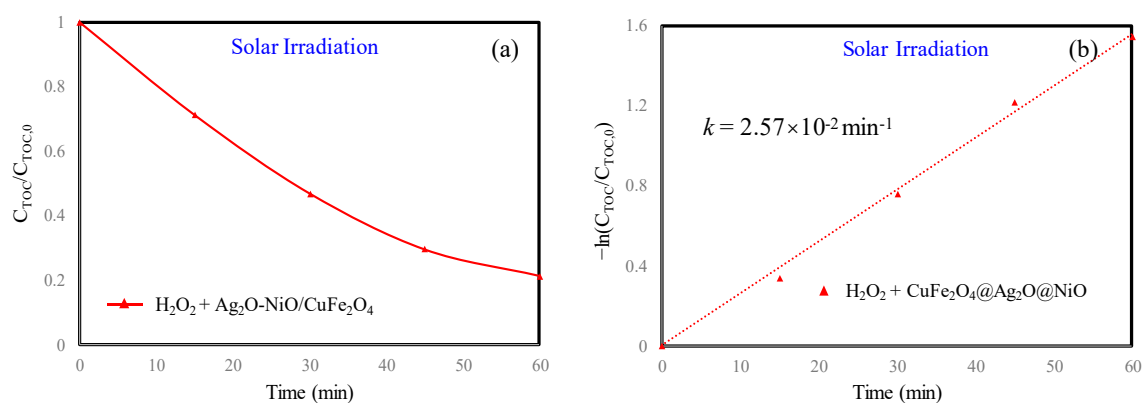

Figure 5. (a) Total organic carbon (TOC) variation of MB; (b) pseudo-first-order kinetic fit for TOC removal during the photo-Fenton process. Initial MB concentration: 10 mg/L. Initial H_2O_2 concentration: 416 mg/L.

By optimizing the amount of catalyst, the unnecessary use of a photocatalyst in degradation experiments could be minimized. For this purpose, the 10 mg/L MB was degraded for 60 min using 1, 5, 10, 20, and 50 mg of catalysts mixed with 100 µL of H_2O_2 in an 80 mL MB solution. The results are shown in Figure 6a,b. It was found that increasing the amount of catalyst from 1 to 50 mg could cause the MB removal rate to increase from 86.06% to 96.67% and then decrease to 81.15%. When the dosage of Ag_2O-$NiO/CuFe_2O_4$ was 10 mg, the catalytic efficiency was the best. When the Ag_2O-$NiO/CuFe_2O_4$ dosage was less than 10 mg, the catalytic efficiency showed a positive correlation with the catalyst dosage. Then, with the further increase of the catalyst dosage, the MB degradation efficiency significantly decreased. When the dosage of catalyst was small, all reaction sites could fully absorb sunlight and participate in the reaction together with H_2O_2 until the dosage of the catalyst reached the optimal value. When the dosage of catalyst excessively increased, the light could not penetrate into the dye solution due to excessive scattering of the material. Thus, the MB degradation in the internal solution was hindered, so the overall degradation effect was poor. When the dosage of Ag_2O-$NiO/CuFe_2O_4$ was 10 mg, the degradation efficiency of MB was positively associated with the dosage of H_2O_2, as shown Figure S3. However, when the dosage of H_2O_2 was greater than 100 µL, the degradation efficiency changed slowly, so 100 µL was the cost-effective dosage for H_2O_2.
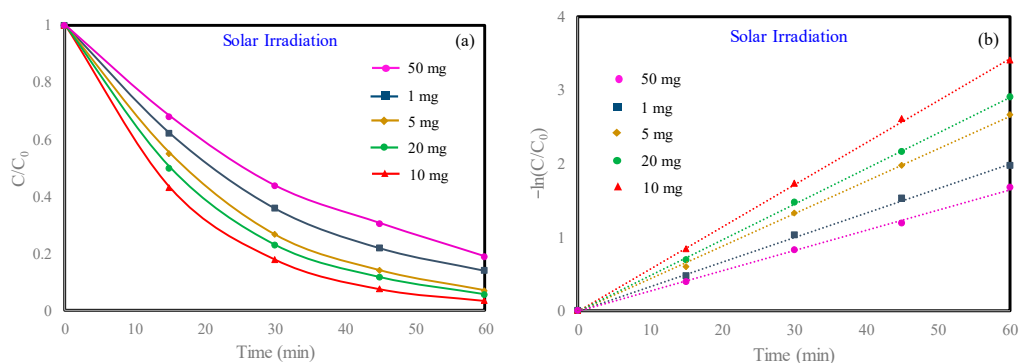
Figure 6. (**a**) Effect of Ag_2O-NiO/$CuFe_2O_4$ dosage on MB dye photodegradation; (**b**) the pseudo-first-order reaction kinetics for MB dye degradation affected by different Ag_2O-NiO/$CuFe_2O_4$ dosages. Initial MB concentration: 10 mg/L. Initial H_2O_2 concentration: 416 mg/L.

3.3. Enhanced Mechanism of Ag_2O-NiO/$CuFe_2O_4$ on Photocatalytic Activity

In order to study the role of ·OH in the MB degradation process, EtOH and TBA were used as ·OH quenchers. Then, we studied their effect on MB degradation, as shown in Figure 7. Both EtOH and TBA inhibited MB degradation. When 10 mL of EtOH and 10 mL of TBA were added, the degradation rates of MB were 0.44% and 0.64%, respectively. These data fully proved that the increase of ·OH produced by the photo-Fenton reaction in this study led to an increase of the MB removal rate.
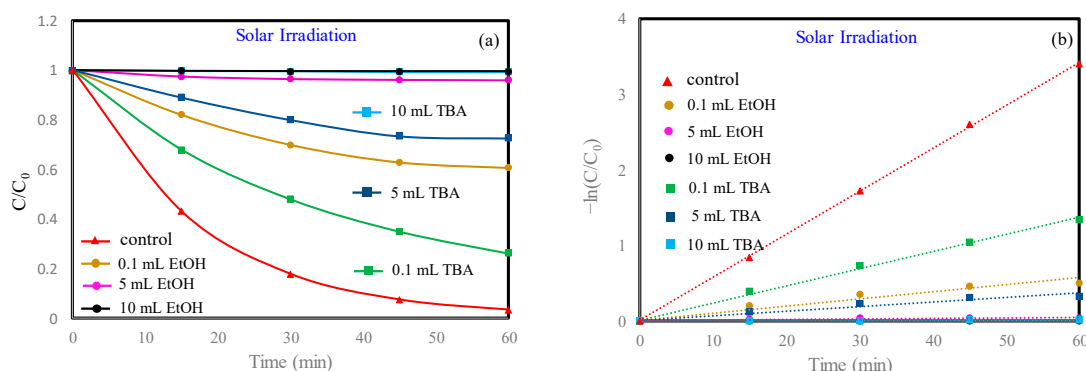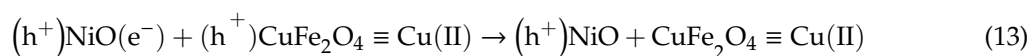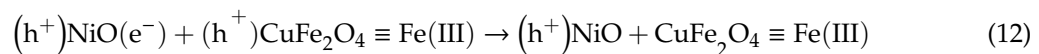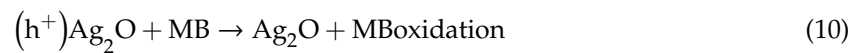

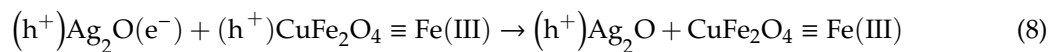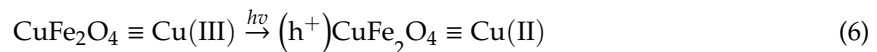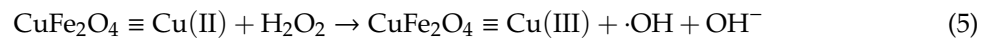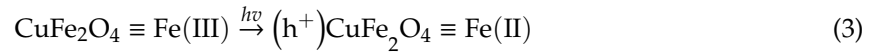**Figure 7.** The impact of different ·OH quenchers on MB removal in a photocatalytic system. (**a**) MB degradation with different quenchers; (**b**) the pseudo-first-order reaction kinetics for MB degradation with different quenchers. Initial MB concentration: 10 mg/L. Initial H_2O_2 concentration: 416 mg/L.

Ag_2O-NiO/$CuFe_2O_4$ showed an excellent photocatalytic performance. Ag_2O-NiO/$CuFe_2O_4$ was much more efficient in degrading MB than $CuFe_2O_4$. $CuFe_2O_4$ was a typical photocatalytic semiconductor material with band gap width E_g = 1.43 eV, a conduction band bottom position E_c = −1.12 V, and a valence band top position E_v = 0.31 V [31]. Under the sunlight irradiation, electrons in the valence band of $CuFe_2O_4$ could absorb the photons (hv > 1.43 eV) and jump to the conduction band. Photogenerated electrons have reductive properties [32]. Thus, the ferric iron Fe(III) in $CuFe_2O_4$ can be reduced to Fe(II) via a ligand-to-metal charge transfer (LMCT) mechanism. As such, Fe(II) and Cu(II) all can catalytically decompose H_2O_2 into OH, which is the key active species to degrade MB dye [33]. Here, MB was adsorbed onto the surface of photocatalytic material due to hydrogen bonding, π–π interactions, surface complexation, electrostatic interactions, and chemisorption. Then, the Fe(III) and Cu(III) generated by H_2O_2 oxidation could be reduced into Fe(II) and Cu(II) by photo-induced electrons, but the $CuFe_2O_4$ would show an oxidation state because it lacked electron, thus resulting in a low photo-Fenton efficiency. The photo-Fenton reaction process sponsored by $CuFe_2O_4$ can be described by Equations (3)–(6) [13].

Ag$_2$O and NiO are commonly used as photocatalysts. Ag$_2$O has a narrow band gap, E$_g$ = 1.51 eV, and electron-hole pairs can be generated by absorbing visible light [13]. NiO has a wide band gap width of 3.63 eV. The bottom of NiO conduction band is E$_c$ = −0.345 V, and the top of the valence band is E$_v$ = 3.285 V [34]. A ternary catalyst composed of Ag$_2$O, NiO, and CuFe$_2$O$_4$ can greatly improve photocatalytic efficiency.

$$CuFe_2O_4 \equiv Fe(III) \xrightarrow{h\nu} \left(h^+\right)CuFe_2O_4 \equiv Fe(II) \tag{3}$$

$$\left(h^+\right)CuFe_2O_4 \equiv Fe(II) + H_2O_2 \rightarrow (h^+)CuFe_2O_4 \equiv Fe(III) + \cdot OH + OH^- \tag{4}$$

$$CuFe_2O_4 \equiv Cu(II) + H_2O_2 \rightarrow CuFe_2O_4 \equiv Cu(III) + \cdot OH + OH^- \tag{5}$$

$$CuFe_2O_4 \equiv Cu(III) \xrightarrow{h\nu} \left(h^+\right)CuFe_2O_4 \equiv Cu(II) \tag{6}$$

$$Ag_2O \xrightarrow{h\nu} \left(h^+\right)Ag_2O(e^-) \tag{7}$$

$$\left(h^+\right)Ag_2O(e^-) + (h^+)CuFe_2O_4 \equiv Fe(III) \rightarrow \left(h^+\right)Ag_2O + CuFe_2O_4 \equiv Fe(III) \tag{8}$$

$$\left(h^+\right)Ag_2O(e^-) + (h^+)CuFe_2O_4 \equiv Cu(II) \rightarrow \left(h^+\right)Ag_2O + CuFe_2O_4 \equiv Cu(II) \tag{9}$$

$$\left(h^+\right)Ag_2O + MB \rightarrow Ag_2O + MBoxidation \tag{10}$$

$$NiO \xrightarrow{h\nu} (h+)NiO(e^-) \tag{11}$$

$$\left(h^+\right)NiO(e^-) + (h^+)CuFe_2O_4 \equiv Fe(III) \rightarrow \left(h^+\right)NiO + CuFe_2O_4 \equiv Fe(III) \tag{12}$$

$$\left(h^+\right)NiO(e^-) + (h^+)CuFe_2O_4 \equiv Cu(II) \rightarrow \left(h^+\right)NiO + CuFe_2O_4 \equiv Cu(II) \tag{13}$$

$$\left(h^+\right)NiO + OH^- \rightarrow NiO + \cdot OH \tag{14}$$

$$\cdot OH + MB \rightarrow CO_2 + H_2O + \ldots\ldots \tag{15}$$

Because the number of photoelectrons produced by CuFe$_2$O$_4$ is very limited and the Fe(III) and Cu(III) cannot be reduced in time, the photo-Fenton degradation effect of MB by the pristine CuFe$_2$O$_4$ reaction was very poor. Ag$_2$O and NiO were able to promote the transition of photoelectrons in the ternary catalyst, as shown in Figure 8. The electrons in the valence band could jump into the conduction band under the sunlight excitation in Ag$_2$O and NiO. Then, these photo-induced electrons could jump into the valence band of CuFe$_2$O$_4$ via a heterogeneous structure, thus promoting the effective reduction for Fe(III) and Cu(III) in CuFe$_2$O$_4$ and further improving the photo-Fenton efficiency. In addition, the photo-induced hole in Ag$_2$O could also directly oxidatively degrade MB. Meanwhile, the photo-induced hole in NiO could oxidize OH$^-$ or H$_2$O to produce OH for MB degradation [35].
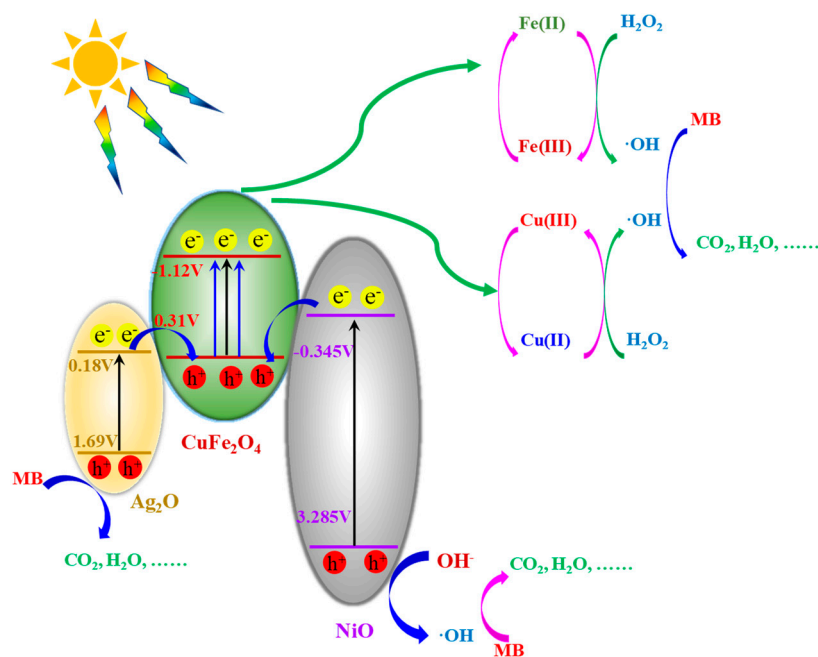
Figure 8. The proposed mechanism for enhanced photo-Fenton reactions with the ternary catalyst Ag_2O-NiO/$CuFe_2O_4$.

4. Conclusions

Ag_2O-NiO/$CuFe_2O_4$ was synthesized by simple hydrothermal and calcination methods, and its morphology and structure characteristics were analyzed by TEM and XRD. The synthesized Ag_2O-NiO/$CuFe_2O_4$ showed an excellent catalytic performance in the degradation of MB in wastewater via the photo-Fenton reaction. The mineralization rate of the 10 mg/L (80 mL) MB solution was 78.64% within 60 min with 10 mg of the Ag_2O-NiO/$CuFe_2O_4$ photo-Fenton catalyst and 100 μL of H_2O_2. The novelty of this study lies in that Ag_2O-NiO/$CuFe_2O_4$ is a novel, simple, low-cost and high-efficient photocatalyst.

References

1. Arshad, H.; Imran, M.; Ashraf, M. Toxic effects of Red-S3B dye on soil microbial activities, wheat yield, and their alleviation by pressmud application. *Ecotoxicol. Environ. Saf.* **2020**, *204*, 111030. [CrossRef] [PubMed]

2. Gebrezgiher, M.; Kiflie, Z. Utilization of cactus peel as biosorbent for the removal of reactive dyes from textile dye effluents. *J. Environ. Public Health* **2020**, *2020*, 5383842. [CrossRef] [PubMed]

3. Al-Baldawi, I.A.; Abdullah, S.R.S.; Anuar, N.; Hasan, H.A. Phytotransformation of methylene blue from water using aquatic plant (*Azolla pinnata*). *Environ. Technol. Innov.* **2018**, *11*, 15–22. [CrossRef]

4. Sargin, I.; Baran, T.; Arslan, G. Environmental remediation by chitosan-carbon nanotube supported palladium nanoparticles: Conversion of toxic nitroarenes into aromatic amines, degradation of dye pollutants and green synthesis of biaryls. *Sep. Purif. Technol.* **2020**, *247*, 116987. [CrossRef]

5. Liu, L.; Li, S.; An, Y.; Sun, X.; Wu, H.; Li, J.; Chen, X.; Li, H. Hybridization of nanodiamond and CuFe-LDH as heterogeneous photoactivator for visible-light driven photo-fenton reaction: Photocatalytic activity and mechanism. *Catalysts* **2019**, *9*, 118. [CrossRef]

6. Belghit, A.; Merouani, S.; Hamdaoui, O.; Alghyamah, A.; Bouhelassa, M. Influence of processing conditions on the synergism between UV irradiation and chlorine toward the degradation of refractory organic pollutants in UV/chlorine advanced oxidation system. *Sci. Total Environ.* **2020**, *736*, 139623. [CrossRef]

7. Ali, A.; Ing, A.W.C.; Abdullah, W.R.W.; Hamzah, S.; Azaman, F. Preparation of high-performance adsorbent from low-cost agricultural waste (Peanut husk) using full factorial design: Application to dye removal. *Biointerface Res. Appl. Chem.* **2020**, *10*, 6619–6628.

8. Thiruppathi, M.; Leeladevi, K.; Ramalingan, C.; Chen, K.-C.; Nagarajan, E.R. Construction of novel biochar supported copper tungstate nanocomposites: A fruitful divergent catalyst for photocatalysis and electrocatalysis. *Mater. Sci. Semicond. Process.* **2020**, *106*, 104766. [CrossRef]

9. Liu, J.; Tao, Z.; Xie, H.; Zhang, X.; Wang, H.; Xiao, H.; Wang, L. Facial construction of defected NiO/TiO_2 with Z-scheme charge transfer for enhanced photocatalytic performance. *Catal. Today* **2019**, *335*, 269–277. [CrossRef]

10. Lyu, J.; Ge, M.; Hu, Z.; Guo, C. One-Pot synthesis of magnetic $CuO/Fe_2O_3/CuFe_2O_4$ nanocomposite to activate persulfate for levofloxacin removal: Investigation of efficiency, mechanism and degradation route. *Chem. Eng. J.* **2020**, *389*, 124456. [CrossRef]

11. Ren, J.; Zhu, Y. Ag_2O-decorated electrospun $BiVO_4$ nanofibers with enhanced photocatalytic performance. *RSC Adv.* **2020**, *10*, 6114–6120. [CrossRef]

12. Qin, Y.; Li, H.; Lu, J.; Feng, Y.; Meng, F.; Ma, C.; Yan, Y.; Meng, M. Synergy between van der waals heterojunction and vacancy in $ZnIn_2S_4/g-C_3N_4$ 2D/2D photocatalysts for enhanced photocatalytic hydrogen evolution. *Appl. Catal. B Environ.* **2020**, *277*, 119254. [CrossRef]

13. Du, X.; Liu, L.; Dong, Z.; Cui, Z.; Sun, X.; Wu, D.; Ma, Z.; Fang, Z.; Liu, Y.; An, Y. Accelerated redox cycles of Fe(III)/Fe(II) and Cu(III)/Cu(II) by photo-induced electron from N-CQDs for enhanced photo-fenton capability of CuFe-LDH. *Catalysts* **2020**, *10*, 960. [CrossRef]

14. Samson, V.A.F.; Bernadsha, S.B.; Mahendiran, M.; Lawrence, K.L.; Madhavan, J.; Raj, M.V.A.; Prathap, S. Impact of calcination temperature on structural, optical, and magnetic properties of spinel $CuFe_2O_4$ for enhancing photocatalytic activity. *J. Mater. Sci. Mater. Electron.* **2020**, *31*, 6574–6585. [CrossRef]

15. Li, Z.; Guo, C.; Lyu, J.; Hu, Z.; Ge, M. Tetracycline degradation by persulfate activated with magnetic $Cu/CuFe_2O_4$ composite: Efficiency, stability, mechanism and degradation pathway. *J. Hazard. Mater.* **2019**, *373*, 85–96. [CrossRef]

16. Li, J.; Ren, Y.; Ji, F.; Lai, B. Heterogeneous catalytic oxidation for the degradation of p-nitrophenol in aqueous solution by persulfate activated with $CuFe_2O_4$ magnetic nano-particles. *Chem. Eng. J.* **2017**, *324*, 63–73. [CrossRef]

17. Tarek, M.; Rezaul Karim, K.M.; Sarkar, S.M.; Deb, A.; Ong, H.R.; Abdullah, H.; Cheng, C.K.; Rahman Khan, M.M. Hetero-Structure $CdS–CuFe_2O_4$ as an efficient visible light active photocatalyst for photoelectrochemical reduction of CO_2 to methanol. *Int. J. Hydrogen Energy* **2019**, *44*, 26271–26284. [CrossRef]

18. Karunakaran, C.; Sakthiraadha, S.; Gomathisankar, P.; Vinayagamoorthy, P. Nanostructures and optical, electrical, magnetic, and photocatalytic properties of hydrothermally and sonochemically prepared $CuFe_2O_4/SnO_2$. *RSC Adv.* **2013**, *3*, 16728. [CrossRef]

19. Guo, Y.; Zhang, L.; Liu, X.; Li, B.; Tang, D.; Liu, W.; Qin, W. Synthesis of magnetic core-shell carbon dot@MFe_2O_4 (M = Mn, Zn and Cu) hybrid materials and their catalytic properties. *J. Mater. Chem. A* **2016**, *4*, 4044–4055. [CrossRef]

20. Guo, W.; Zou, J.; Guo, B.; Xiong, J.; Liu, C.; Xie, Z.; Wu, L. Pd nanoclusters/TiO_2(B) nanosheets with surface defects toward rapid photocatalytic dehalogenation of polyhalogenated biphenyls under visible light. *Appl. Catal. B Environ.* **2020**, *277*, 119255. [CrossRef]

21. Bai, X.; Wang, X.; Lu, X.; Liang, Y.; Li, J.; Wu, L.; Li, H.; Hao, Q.; Ni, B.J.; Wang, C. Surface defective g-C_3N_4-xClx with unique spongy structure by polarization effect for enhanced photocatalytic removal of organic pollutants. *J. Hazard. Mater.* **2020**, *398*, 122897. [CrossRef] [PubMed]

22. Su, J.; Yu, S.; Xu, M.; Guo, Y.; Sun, X.; Fan, Y.; Zhang, Z.; Yan, J.; Zhao, W. Enhanced visible light photocatalytic performances of few-layer MoS_2@TiO_2 hollow spheres heterostructures. *Mater. Res. Bull.* **2020**, *130*, 110936. [CrossRef]

23. Yang, H.; Fan, J.; Zhou, C.; Luo, R.; Liu, H.; Wan, Y.; Zhang, J.; Chen, J.; Wang, G.; Wang, R.; et al. Co_3O_4@CdS hollow spheres derived from ZIF-67 with a high phenol and dye photodegradation activity. *ACS Omega* **2020**, *5*, 17160–17169. [CrossRef] [PubMed]

24. Ma, Q.; Zhang, X.; Guo, R.; Zhang, H.; Cheng, Q.; Xie, M.; Cheng, X. Persulfate activation by magnetic γ-Fe_2O_3/Mn_3O_4 nanocomposites for degradation of organic pollutants. *Sep. Purif. Technol.* **2019**, *210*, 335–342. [CrossRef]

25. Pakzad, K.; Alinezhad, H.; Nasrollahzadeh, M. Green synthesis of Ni@Fe_3O_4 and CuO nanoparticles using Euphorbia maculata extract as photocatalysts for the degradation of organic pollutants under UV-irradiation. *Ceram. Int.* **2019**, *45*, 17173–17182. [CrossRef]

26. Zhang, X.; Lin, Q.; Luo, H.; Huang, R.; Xiao, R.; Liu, Q. Activation of persulfate with 3D urchin-like CoO-CuO microparticles for DBP degradation: A catalytic mechanism study. *Sci. Total Environ.* **2019**, *655*, 614–621. [CrossRef]

27. Mohaghegh, N.; Kamrani, S.; Tasviri, M.; Elahifard, M.; Gholami, M. Nanoporous Ag_2O photocatalysts based on copper terephthalate metal-organic frameworks. *J. Mater. Sci.* **2015**, *50*, 4536–4546. [CrossRef]

28. Kannan, K.; Radhika, D.; Nikolova, M.P.; Sadasivuni, K.K.; Mahdizadeh, H.; Verma, U. Structural studies of bio-mediated NiO nanoparticles for photocatalytic and antibacterial activities. *Inorg. Chem. Commun.* **2020**, *113*, 107755. [CrossRef]

29. Taheri-Ledari, R.; Valadi, K.; Gharibi, S.; Maleki, A. Synergistic photocatalytic effect between green LED light and Fe_3O_4/ZnO-modified natural pumice: A novel cleaner product for degradation of methylene blue. *Mater. Res. Bull.* **2020**, *130*, 110946. [CrossRef]

30. Yang, S.; Xu, D.; Chen, B.; Luo, B.; Yan, X.; Xiao, L.; Shi, W. Synthesis and visible-light-driven photocatalytic activity of p–n heterojunction Ag_2O/$NaTaO_3$ nanocubes. *Appl. Surf. Sci.* **2016**, *383*, 214–221. [CrossRef]

31. Cao, Y.; Fang, Y.; Lei, X.Y.; Tan, B.H.; Hu, X.; Liu, B.J.; Chen, Q.L. Fabrication of novel $CuFe_2O_4$/MXene hierarchical heterostructures for enhanced photocatalytic degradation of sulfonamides under visible light. *J. Hazard. Mater.* **2020**, *387*, 122021. [CrossRef] [PubMed]

32. Ohtani, B. Revisiting the fundamental physical chemistry in heterogeneous photocatalysis: Its thermodynamics and kinetics. *Phys. Chem. Chem. Phys.* **2014**, *16*, 1788–1797. [CrossRef] [PubMed]

33. Schneider, J.; Matsuoka, M.; Takeuchi, M.; Zhang, J.L.; Horiuchi, Y.; Anpo, M.; Bahnemann, D.W. Understanding TiO 2 photocatalysis: Mechanisms and materials. *Chem. Rev.* **2014**, *114*, 9919–9986. [CrossRef] [PubMed]

34. Munawar, T.; Iqbal, F.; Yasmeen, S.; Mahmood, K.; Hussain, A. Multi metal oxide NiO-CdO-ZnO nanocomposite-synthesis, structural, optical, electrical properties and enhanced sunlight driven photocatalytic activity. *Ceram. Int.* **2020**, *46*, 2421–2437. [CrossRef]

35. Puga, A.V. Photocatalytic production Photocatalytic production of hydrogen from biomass-derived feedstocks. *Coord. Chem. Rev.* **2016**, *315*, 1–66. [CrossRef]